

# Average BLER Analysis of Ambient Backscatter RSMA Systems for URLLC Short-Packet Communications

Anh-Thu PHAM<sup>1</sup>, Sang-Quang NGUYEN<sup>2</sup>, Phu-Nguyen LE<sup>3</sup>,  
Hai-Trieu LE<sup>4</sup>, Minh-Tuan DANG<sup>5</sup>, Trong-Minh HOANG<sup>1,\*</sup>

<sup>1</sup> Posts and Telecommunications Institute of Technology, Hanoi, Vietnam

<sup>2</sup> Posts and Telecommunications Institute of Technology, Ho Chi Minh City, Vietnam

<sup>3</sup> Faculty of Engineering and Technology, Nguyen Tat Thanh University, Ho Chi Minh City, Vietnam

<sup>4</sup> Institute of Science and Technology, MoPS Vietnam, Hanoi, Vietnam

<sup>5</sup> CMC University, Hanoi, Vietnam

\* hoangtrongminh@ptit.edu.vn

Submitted August 17, 2025 / Accepted October 26, 2025 / Online first November 10, 2025

**Abstract.** *Rate-splitting multiple access (RSMA) has emerged as a promising approach for ultra-reliable and low-latency communications (URLLC), addressing stringent delay and reliability requirements in next-generation networks. This study investigates downlink RSMA for URLLC short-packet communication (SPC) by analyzing the average block error rate (BLER) in an RSMA-enabled symbiotic backscatter system. A base station serving two users via RSMA is considered, while a backscatter device passively assists the transmission, improving overall efficiency. Closed-form expressions are derived for approximate BLERs and the overall system throughput, and validated through Monte Carlo simulations. Results indicate that RSMA achieves about one order-of-magnitude lower BLER than NOMA at  $p_S = 30$  dB and approximately 15–20% higher throughput in the considered short-packet regime. The impact of power allocation and blocklength on reliability is also investigated, providing design insights for URLLC optimization. These findings demonstrate that RSMA offers improved reliability and fairness under envisioned URLLC short-packet scenarios, while the inclusion of passive backscatter enhances energy efficiency without additional transmit power.*

## Keywords

6G, power allocation, rate-splitting multiple access (RSMA), short-packet communication (SPC), symbiotic backscatter radio

## 1. Introduction

The ever-growing demand for wireless communication services has intensified the challenge of spectrum scarcity, driving the development of advanced technologies to optimize spectral efficiency. Among these, non-orthogonal mul-

ti-ple access (NOMA) has emerged as a promising candidate, outperforming traditional orthogonal multiple access (OMA) by enabling more efficient utilization of time and frequency resources. Despite its potential, NOMA faces notable challenges, including complex user pairing, the necessity for signal sharing among users, and fairness concerns arising from successive interference cancellation (SIC) techniques. These limitations hinder its widespread adoption in practical deployments. Although significant efforts have been dedicated to promoting NOMA within next-generation networks through the 3rd Generation Partnership Project (3GPP) [1–3], the emergence of rate-splitting multiple access (RSMA) has begun to eclipse NOMA's relevance.

RSMA addresses many inherent drawbacks of NOMA and offers superior performance [4]. By splitting messages and multiplexing in the power domain at the transmitter, RSMA enables each receiver to decode a common and a private message without learning other users' data, unlike NOMA. These properties make RSMA a strong candidate for 6G, with evidence across joint radar-communications [5], aerial-terrestrial networks [6], reconfigurable intelligent surfaces (RIS) [7], and terahertz (THz) communications [8]. Its practicality has also been demonstrated through prototype implementations [9]. Recent advances have further explored RSMA in UAV-assisted networks, where antenna selection and UAV positioning were optimized to enhance spectral and energy efficiency under both perfect and imperfect SIC [10].

While radio frequency (RF) availability enables cost-effective energy harvesting such as wireless power transfer and simultaneous wireless information and power transfer (SWIPT) [11], these approaches often require non-trivial power budgets, which challenges massive IoT deployments. Therefore, symbiotic radio (SR) has emerged for passive IoT [12], allowing backscatter devices (BDs) to operate parasitically on primary networks and convey data over licensed bands with negligible additional energy.

Recent research has investigated ambient backscatter networks and system-level performance modelling—for example, UAV-assisted directional backscatter communication BackCom with throughput and altitude-range analysis [13] and ambient backscatter cooperative relaying in heterogeneous cognitive radio settings [14]. In [15], the authors proposed RIS-aided MIMO with pilot optimization and channel estimation, which address reliability and resource-efficiency challenges in 6G systems. Complementary to these, [16] analyzed symbiotic backscatter-enabled wireless sensor networks under short-packet communication (SPC), developing a BLER-based framework and revealing how coding gain and packet design affect URLLC reliability. In addition, SPC has been examined in cooperative relay systems with co-channel interference, where optimal power allocation substantially improves BLER and end-to-end throughput over equal-power benchmarks [17]. Related RIS-aided SPC studies have also derived closed-form BLER expressions to ensure reliable and secure content delivery in the presence of untrusted users [18]. Distinct from the above, the present study targets RSMA-enabled symbiotic backscatter under URLLC short-packet constraints and develops tractable reliability characterizations.

Recent studies have explored RSMA and NOMA schemes under various short-packet or backscatter communication settings. Do et al. [16] analyzed a symbiotic backscatter network under SPC and revealed the impact of coding gain and packet design on URLLC reliability. Xu et al. [19] investigated RSMA with finite blocklength constraints and demonstrated superior rate–latency trade-offs compared with NOMA and SDMA, yet without addressing reliability metrics such as BLER. Vu et al. [20] further introduced the concept of symbiotic backscatter RSMA (SB-RSMA) and evaluated its performance via a symbiotic outage probability (SOP) framework. In addition, Abd-Alaziz et al. [21] conducted an exact BER analysis for a coded NOMA system, achieving notable reliability improvements but limited to asymptotic AWGN scenarios. Despite these valuable contributions, none of the aforementioned studies jointly consider finite blocklength, BLER-based reliability evaluation, and the energy-efficiency advantages of passive backscatter. This gap motivates the present study, which develops

a unified analytical framework for RSMA-assisted symbiotic systems under finite blocklength constraints, deriving closed-form BLER and throughput expressions suitable for URLLC short-packet environments.

A concise comparative summary of the aforementioned representative studies is provided in Tab. 1, highlighting their methodologies, performance metrics, and limitations that motivate the present work.

An RSMA-enabled symbiotic backscatter framework is proposed to optimize spectrum usage for next-generation wireless networks. The base station (BS) employs RSMA to serve cellular users (CUs) within the same resource block, while a BD passively encodes its data by adjusting its antenna impedance to backscatter the BS’s RF signal. When the BD is inactive, the system reverts to conventional RSMA. Beyond traditional RSMA and ambient BackCom, the framework targets stringent URLLC requirements—ultra-low latency and high energy efficiency—across cellular and IoT settings [19], [22].

The key contributions of this work are as follows:

- A novel RSMA-enabled symbiotic backscatter system is proposed for future wireless systems, which enhances spectrum efficiency and establishes a sustainable communication model characterised by ultra-low energy consumption—addressing critical energy-efficiency challenges in modern telecommunications.
- Closed-form analytical expressions are derived for *average* BLERs of the common, private, and backscatter streams under quasi-static Rayleigh block fading, enabling comprehensive reliability evaluation and design.
- The effects of power allocation and interference coupling are quantified with respect to URLLC reliability and throughput; with careful resource tuning, RSMA can significantly outperform NOMA, whereas suboptimal allocation may erode these gains.

Based on the above motivations and identified research gaps, the subsequent sections detail the proposed RSMA-enabled symbiotic backscatter model and its comprehensive reliability analysis under finite blocklength constraints.

Reference	Channel model	Performance metric	Main limitation / Contribution to this work
[16] Do et al., 2024	Symbiotic backscatter under SPC	BLER (simulation-based)	No RSMA or FBL; offers initial insight into SPC reliability for URLLC
[19] Xu et al., 2022	RSMA in MISO downlink	Sum-rate vs. blocklength (FBL regime)	Analyzes rate-latency trade-offs; omits BLER and energy aspects
[20] Vu et al., 2024	Symbiotic backscatter RSMA (SB-RSMA)	Symbiotic outage probability (SOP)	Conceptual SB-RSMA via SOP; lacks finite-blocklength reliability study
[21] Abd-Alaziz et al., 2024	Coded NOMA on AWGN	Exact BER (analytical)	Provides exact BER gains (21/17 dB); no fading or FBL analysis
<b>This work</b>	RSMA-enabled symbiotic backscatter (SB-RSMA) under finite blocklength (FBL) URLLC	Average BLER and system throughput (analytical + simulation)	Proposes an analytical SB-RSMA framework; derives closed-form BLER and throughput expressions; demonstrates up to one-order-of-magnitude BLER reduction and 15–20% throughput gain over NOMA.

Tab. 1. Comparative summary of representative works on NOMA/RSMA short-packet studies.

Table 1 clearly highlights that prior RSMA and NOMA studies have not jointly addressed finite blocklength constraints and backscatter-assisted reliability, thereby underscoring the novelty of the present work.

Section 2 details the system and channels; Section 3 develops average BLER/throughput analysis; Section 4 validates and discusses design trends; Section 5 concludes.

## 2. System Model

Figure 1 illustrates a symbiotic communication framework comprising a base station (BS) equipped with a single antenna, two cellular users (CUs), each having a single antenna, and a backscatter device (BD) with signal processing capabilities. The BS communicates with both CUs through RSMA signaling, while the BD engages in passive communication by reflecting and modulating the RF signal it receives from the BS, thus enabling information transfer. The system operates under quasi-stable Rayleigh block fading conditions and employs the same frequency band for both uplink and downlink transmissions.

Let  $\mathcal{K} = \{1, 2\}$  represent the set of CUs, where  $U_k$  denotes the  $k$ -th CU, with  $k \in \mathcal{K}$ . For each fading block, the channel coefficients for the links from BS to BD, from BS to the  $k$ -th CU, and from BD to the  $k$ -th CU are denoted by  $h_0$ ,  $h_k$ , and  $g_k$ , respectively. In a Rayleigh fading environment, the squared magnitudes  $|h_0|^2$ ,  $|h_k|^2$ , and  $|g_k|^2$  are exponentially distributed with parameters  $\lambda_{h_0}$ ,  $\lambda_{h_k}$ , and  $\lambda_{g_k}$ , respectively.

For the sake of clarity, the probability density function (PDF) and cumulative distribution function (CDF) of a generic channel coefficient  $Z \in \{h_0, h_k, g_k\}$  are given by  $f_{|Z|^2}(x) = \frac{1}{\lambda_Z} e^{-x/\lambda_Z}$  and  $F_{|Z|^2}(x) = 1 - e^{-x/\lambda_Z}$ , where  $x \geq 0$  represents the squared magnitude of the channel coefficient, and  $\lambda_Z$  is the corresponding fading parameter for  $Z$ .

In the context of quasi-stable Rayleigh block fading conditions, the channel coefficients  $h_0$ ,  $h_k$ , and  $g_k$  can be readily estimated through two distinct phases of uplink pilot training. During the initial phase, the BD fully captures the signal via reflection, thereby enabling the BS to determine  $h_k$ . Subsequently, in the second phase, the BD transitions into a fixed impedance mode characterized by a predefined symbol  $x_b$ , a backscatter efficiency  $\eta \in (0, 1]$ , and a reflection coefficient  $\delta \in (0, 1]$ . Utilizing the training pilots, the BS is able to compute  $h_0 g_k$  by subtracting  $h_k$  from the composite channel representation  $h_k + \sqrt{\delta\eta} h_0 g_k x_b$ . Ultimately, the parameters  $h_0$  and  $h_k$  are instrumental in the allocation of resources and execution of data decoding at the control units.

### 2.1 Transmission Model

In this model, the BS first separates the messages for the CUs into two categories: common and private components. The common segments, shared across all CUs, are

encoded into a single stream denoted as  $x_c$ , while the private segments, intended for individual users, are encoded into separate streams  $x_k$ , ensuring that  $\mathbb{E}\{|x_c|^2\} = \mathbb{E}\{|x_k|^2\} = 1$  for all  $k$ ,  $\mathbb{E}[\cdot]$  denotes expectation operation. Let  $P_S$  represent the transmission power at the BS, which allocates power factors  $a_c$  and  $a_k$  to the common and private streams, respectively, satisfying the power constraint  $a_c + \sum_{k=1}^K a_k = 1$ . Therefore, the total transmitted signal  $x(t)$  in the  $t$ -th time interval can be expressed as:

$$x(t) = x_c(t)\sqrt{P_S a_c} + \sum_{k=1}^K x_k(t)\sqrt{P_S a_k}. \tag{1}$$

Under the assumption of additive white Gaussian noise (AWGN)  $n_k(t)$  with zero mean and variance  $N_0$ , the received signal at user  $k$ , denoted as  $\bar{y}_k(t)$ , is the result of the direct and backscatter links. It can be written as:

$$\bar{y}_k(t) = h_k x(t) + \sqrt{\delta\eta} h_0 x(t) g_k x_b(t) + n_k(t) \tag{2}$$

where  $h_k$  represents the channel gain from the BS to user  $k$ ,  $h_0$  is the channel gain from the BS to the backscatter device,  $g_k$  is the gain from the backscatter device to user  $k$ , and  $x_b(t)$  is the reflection signal of the backscatter device. The parameters  $\delta$  and  $\eta$  represent the backscatter efficiency and reflection coefficient, respectively, both of which directly impact the overall received signal.

Next, the average signal-to-noise ratio (SNR) is defined as  $\rho_S = \frac{P_S}{N_0}$ . With this, the received signal-to-interference-plus-noise ratio (SINR) for decoding the common stream  $x_c(t)$ , private stream  $x_k(t)$ , and the backscatter stream  $x_b(t)$  are obtained as follows:

$$\begin{aligned} \bar{\gamma}_{k,c} &= \frac{\rho_S a_c |h_k|^2}{\rho_S a_k |h_k|^2 + \delta\eta\rho_S |h_0|^2 |g_k|^2 + 1}, \\ \bar{\gamma}_{k,k} &= \frac{\rho_S a_k |h_k|^2}{\delta\eta\rho_S |h_0|^2 |g_k|^2 + 1}, \\ \bar{\gamma}_{k,b} &= \delta\eta\rho_S |h_0|^2 |g_k|^2. \end{aligned} \tag{3}$$

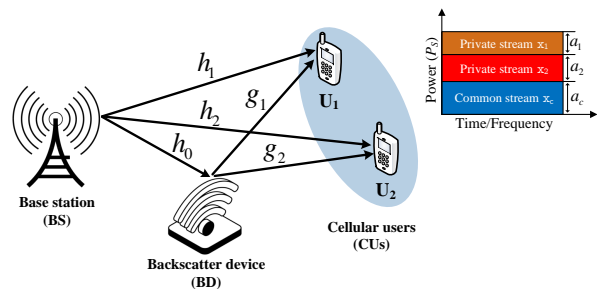


Fig. 1. System architecture of a downlink RSMA-enabled network with ambient backscatter communication support.

To enhance the readability and reproducibility of the mathematical model, the overall signal processing flow of the RSMA-enabled symbiotic backscatter system can be summarized as follows: i) the BS generates a superimposed RSMA signal composed of one common and two private streams as in (1); ii) the BD reflects and modulates the received waveform according to its impedance state, producing the composite signal at each CU as formulated in (2); iii) each CU performs successive decoding of the common, private, and backscatter components based on the SINRs in (3). This concise formulation helps future researchers share, implement, and extend the analytical model for comparative studies.

## 2.2 Channel Characteristics

In this subsection, the PDF and CDF for the product of two channel gains  $h_0$  and  $g_k$  are analyzed, which are denoted as  $f_{|h_0|^2|g_k|^2}(x)$  and  $F_{|h_0|^2|g_k|^2}(x)$ , respectively, as derived in [23], [24]. The expressions for the PDF and CDF are given by:

$$f_{|h_0|^2|g_k|^2}(x) = \frac{2}{\lambda_{h_0}\lambda_{g_k}} K_0 \left( 2\sqrt{\frac{x}{\lambda_{h_0}\lambda_{g_k}}} \right), \quad (4a)$$

$$F_{|h_0|^2|g_k|^2}(x) = 1 - 2\sqrt{\frac{x}{\lambda_{h_0}\lambda_{g_k}}} K_1 \left( 2\sqrt{\frac{x}{\lambda_{h_0}\lambda_{g_k}}} \right) \quad (4b)$$

where  $K_a(\cdot)$  denotes the modified Bessel function of the second kind of order  $a$ .

For analytical compactness, an auxiliary mapping function  $\mathcal{G}(z)$  is introduced to express the CDF of  $\Delta_k$  in a unified form for both the common and private streams. Next, the of  $\Delta_k$ , where  $\Delta_k \in \{\tilde{\gamma}_{k,c}, \tilde{\gamma}_{k,b}\}$ , is determined as shown in (5). Here,  $\mathcal{G}(z) \in \left\{ \frac{z}{\rho_S(a_c - za_k)}, \frac{z}{\rho_S a_k} \right\}$ .

$$\begin{aligned} F_{\Delta_k}(z) &= 1 - \Pr(\Delta_k > z) \\ &= 1 - \Pr\left(|h_k|^2 > \mathcal{G}(z)(\delta\eta\rho_S|h_0|^2|g_k|^2 + 1)\right) \end{aligned} \quad (5)$$

which simplifies to:

$$\begin{aligned} F_{\Delta_k}(z) &= 1 - \int_0^{+\infty} f_{|h_0|^2|g_k|^2}(y) \\ &\quad \times \left[ 1 - F_{|h_k|^2}(\mathcal{G}(z)(\delta\eta\rho_S y + 1)) \right] dy. \end{aligned}$$

For compactness, the integral term associated with the exponential-Bessel kernel is denoted by  $A$ , which will be further evaluated in closed form using polynomial expansion techniques. By substituting (4a) and the CDF of  $|h_k|^2$  into (5),  $F_{\Delta_k}(z)$  can be obtained as:

$$F_{\Delta_k}(z) = 1 - \underbrace{\frac{2e^{-\frac{\mathcal{G}(z)}{\lambda_{h_k}}}}{\lambda_{h_0}\lambda_{g_k}} \int_0^{\infty} e^{-\frac{\delta\eta\rho_S\mathcal{G}(z)}{\lambda_{h_k}}x} K_0 \left( 2\sqrt{\frac{x}{\lambda_{h_0}\lambda_{g_k}}} \right) dx}_{A} \quad (6)$$

Note that  $A$  in (6) depends on the auxiliary function  $\mathcal{G}(z)$ , which links the fading parameters to the SNR threshold  $z$ . This dependence will be retained in the subsequent closed-form expansion.

Using [25, Eq. (6.614.4)] and applying polynomial expansion techniques,  $A$  is expressed as:

$$\begin{aligned} A &= \frac{e^{\frac{\Xi_k}{2\mathcal{G}(z)}}}{2\sqrt{\frac{\delta\eta\rho_S\mathcal{G}(z)}{\lambda_{h_0}\lambda_{h_k}\lambda_{g_k}}}} W_{-\frac{1}{2},0} \left( \frac{\Xi_k}{\mathcal{G}(z)} \right) \\ &= \frac{e^{\frac{\Xi_k}{2\mathcal{G}(z)}} e^{-\frac{\Xi_k}{2\mathcal{G}(z)}}}{2\sqrt{\frac{\delta\eta\rho_S\mathcal{G}(z)}{\lambda_{h_0}\lambda_{h_k}\lambda_{g_k}}}} \sqrt{\frac{\Xi_k}{\mathcal{G}(z)}} U \left( 1, 1, \frac{\Xi_k}{\mathcal{G}(z)} \right) \\ &= \frac{e^{\frac{\Xi_k}{2\mathcal{G}(z)}} e^{-\frac{\Xi_k}{2\mathcal{G}(z)}}}{2\sqrt{\frac{\delta\eta\rho_S\mathcal{G}(z)}{\lambda_{h_0}\lambda_{h_k}\lambda_{g_k}}}} \sqrt{\frac{\Xi_k}{\mathcal{G}(z)}} e^{\frac{\Xi_k}{\mathcal{G}(z)}} \text{Ei} \left( -\frac{\Xi_k}{\mathcal{G}(z)} \right) \\ &= -\frac{\lambda_{h_k} e^{\frac{\Xi_k}{\mathcal{G}(z)}}}{2\delta\eta\rho_S\mathcal{G}(z)} \text{Ei} \left( -\frac{\Xi_k}{\mathcal{G}(z)} \right) \end{aligned} \quad (7)$$

where  $\Xi_k = \frac{\lambda_{h_k}}{\lambda_{h_0}\lambda_{g_k}\delta\eta\rho_S}$ ,  $W_{\lambda,\mu}(z)$  is the Whittaker function defined as  $W_{\lambda,\mu}(z) = e^{-\frac{z}{2}} z^{\mu+\frac{1}{2}} U \left( \mu - \lambda + \frac{1}{2}, 1 + 2\mu; z \right)$ , where  $U(\mu, k; z)$  is the confluent hypergeometric function defined as  $U(\mu, k; z) = \frac{1}{\Gamma(\mu)} \int_0^{\infty} e^{-zt} t^{\mu-1} (1+t)^{k-\mu-1} dt$ ,  $\mu > 0$ , and  $\text{Ei}(-x)$  is the exponential integral function defined as  $\text{Ei}(-x) = \int_{-\infty}^x e^p p^{-1} dp$ .

By substituting (7) into (6) and performing the necessary algebraic manipulations, the CDF of  $\Delta_k$  is obtained as:

$$F_{\Delta_k}(z) = 1 + \frac{\Xi_k e^{\frac{\Xi_k}{\mathcal{G}(z)} - \frac{\mathcal{G}(z)}{\lambda_{h_k}}}}{\mathcal{G}(z)} \text{Ei} \left( -\frac{\Xi_k}{\mathcal{G}(z)} \right). \quad (8)$$

Finally, the CDF of  $\tilde{\gamma}_{k,b}$  is expressed as:

$$\begin{aligned} F_{\tilde{\gamma}_{k,b}}(z) &= 1 - \Pr(\tilde{\gamma}_{k,b} > z) \\ &= F_{|h_0|^2|g_k|^2} \left( \frac{z}{\delta\eta\rho_S} \right) \\ &= 1 - 2\sqrt{\frac{z}{\lambda_{h_0}\lambda_{g_k}\delta\eta\rho_S}} K_1 \left( 2\sqrt{\frac{z}{\lambda_{h_0}\lambda_{g_k}\delta\eta\rho_S}} \right). \end{aligned} \quad (9)$$

For clarity, the key notations and parameters used throughout this paper are summarized in Tab. 2.

Symbol	Description
$P_S$	Transmit power at the source node
$\rho_S$	Transmit signal-to-noise ratio (SNR) in dB
$a_1, a_2$	Power allocation factors for common and private streams
$\delta$	Efficiency coefficient of the backscatter link
$\eta$	Reflection coefficient of the backscatter device (BD)
$\mathcal{L}$	Blocklength (number of channel uses)
$R_1, R_2$	Transmission rate at $U_1$ and $U_2$
$\bar{\gamma}_i$	Instantaneous SINR of user $i$
$N_0$	Noise power spectral density
$h_0, g_1, g_2, h_1, h_2$	Channel coefficients between BS, BD, and users
$\lambda_{h_0}, \lambda_{h_1}, \lambda_{h_2}, \lambda_{g_1}, \lambda_{g_2}$	Average channel gains of corresponding links
$\mathcal{T}_1, \mathcal{T}_2, \mathcal{T}_c$	Number of information bits
$\bar{\epsilon}_{U_i}$	Average BLER of user $U_i$

Tab. 2. Summary of key notations used in this paper.

### 3. Average BLER Analysis

The mathematical model developed in Sec. 2 is analytically shared here through a tractable framework linking the SINR statistics in (3)–(9) to the average BLER expressions in (10)–(18), ensuring that each analytical step is interpretable and reproducible for future benchmarking.

In this section, a comprehensive examination of the average BLER pertaining to the proposed system is conducted. For the sake of clarity and operational convenience, the notation  $R_i$  bit/s/Hz, where  $i$  is an element of the set  $\{c, 1, 2\}$ , is used to represent the utmost attainable rate for the variable  $x_i$ , which is contingent upon a defined block length of  $\mathcal{L}_i$  bits. Given that the blocklength is sufficiently large, specifically ( $\mathcal{L}_i \geq 100$  bits) as indicated in [26], the instantaneous BLER corresponding to the SINR  $\bar{\gamma}_m$  ( $m \in \{\{1, c\}, \{2, c\}, \{1, k\}, \{2, k\}, \{1, b\}, \{2, b\}\}$ ) can be formulated as:

$$\epsilon_m = Q \left( \frac{C(\bar{\gamma}_m) - R_i}{\sqrt{\mathcal{V}(\bar{\gamma}_m)/\mathcal{L}_i}} \right) \quad (10)$$

where  $R_i = \mathcal{T}_i/\mathcal{L}_i$ , in which  $\mathcal{T}_i$  and  $\mathcal{L}_i$  denote the number of information bits and the transmit blocklength for  $U_1, U_2$ , and the BD when decoding  $x_i$ , respectively. The channel dispersion is  $\mathcal{V}(\bar{\gamma}_m) = [1 - (1 + \bar{\gamma}_m)^{-2}]/(\ln 2)^2$ , the Shannon capacity is  $C(\bar{\gamma}_m) = \log_2(1 + \bar{\gamma}_m)$ , and  $Q(\cdot)$  denotes the Gaussian Q-function. Since obtaining a closed-form expression for  $\epsilon_m$  in (10) is intractable, a tight linear approximation from [27] is adopted to approximate the Q-function, expressed as

$$\epsilon_m = \begin{cases} 1 & \bar{\gamma}_m < \alpha_i \\ 0.5 - \chi_i \sqrt{\mathcal{L}_i} (\bar{\gamma}_m - \gamma_{th,i}) & \bar{\gamma}_m \in [\alpha_i, \beta_i] \\ 0 & \bar{\gamma}_m > \beta_i \end{cases} \quad (11)$$

Then, the average BLER  $\bar{\epsilon}_m \triangleq \mathbb{E}[\epsilon_m]$  is computed as [28, Eq. (13)]:

$$\bar{\epsilon}_m = \int_0^\infty \epsilon_m(x) f_{\bar{\gamma}_m}(x) dx = \chi_i \sqrt{\mathcal{L}_i} \int_{\alpha_i}^{\beta_i} F_{\bar{\gamma}_m}(x) dx. \quad (12)$$

In the context of the successive interference cancellation approach employed in RSMA, the user  $U_k$  is required to sequentially decode three distinct messages, namely,  $x_c(t)$ ,  $x_k(t)$ , and  $x_b(t)$ , with the assistance of SIC techniques. Consequently, the overall BLER for user  $U_k$  is contingent upon the BLERs associated with user  $U_k$ 's decoding of the three messages  $x_c(t)$ ,  $x_k(t)$ , and  $x_b(t)$ . Given that the reliability threshold in ultra-reliable low-latency communication is notably stringent (e.g., ranging from  $10^{-5}$  to  $10^{-9}$ ), the multiplicative term of the two error probabilities can be disregarded. Consequently, the average BLER of  $U_k$  can be approximated as

$$\bar{\epsilon}_{U_k} \approx \bar{\epsilon}_{k,c} + \bar{\epsilon}_{k,k} + \bar{\epsilon}_{k,b}. \quad (13)$$

By combining (8) and (12), the average BLER of  $\bar{\epsilon}_{k,c}$  and  $\bar{\epsilon}_{k,k}$  can be derived as:

$$\begin{aligned} \bar{\epsilon}_\ell &= \chi_\ell \sqrt{\mathcal{L}_\ell} \int_{\alpha_\ell}^{\beta_\ell} F_{\Delta_k}(x) dx \\ &= 1 + \chi_\ell \sqrt{\mathcal{L}_\ell} \Xi_k \int_{\alpha_\ell}^{\beta_\ell} \frac{e^{\frac{\Xi_k}{\mathcal{G}(x)} - \frac{\mathcal{G}(x)}{\lambda_{h_k}}}}{\mathcal{G}(x)} dx \\ &\quad \times \text{Ei} \left( -\frac{\Xi_k}{\mathcal{G}(x)} \right). \end{aligned} \quad (14)$$

Here,  $\ell = c$  if  $\iota = \{k, c\}$  and  $\ell = 1$  if  $\iota = \{k, k\}$ . While deriving a closed-form expression for (14) is challenging, a precise approximation can be achieved by utilizing the Gaussian-Chebyshev quadrature [29, Eq. (25.4.38)], yielding

$$\begin{aligned} \bar{\epsilon}_\ell &\approx 1 + \frac{\chi_\ell \sqrt{\mathcal{L}_\ell} \Xi_k (\beta_\ell - \alpha_\ell) \pi}{2Q} \\ &\quad \times \sum_{q=1}^Q \left| \sin \frac{(2q-1)\pi}{2Q} \right| \frac{e^{\frac{\Xi_k}{\mathcal{G}(\zeta_q)} - \frac{\mathcal{G}(\zeta_q)}{\lambda_{h_k}}}}{\mathcal{G}(\zeta_q)} \\ &\quad \times \text{Ei} \left( -\frac{\Xi_k}{\mathcal{G}(\zeta_q)} \right) \end{aligned} \quad (15)$$

where  $Q$  is a trade-off parameter between accuracy and complexity and  $\zeta_q = \frac{0.5}{\chi_\ell \sqrt{\mathcal{L}_\ell}} \cos \left( \frac{(2q-1)\pi}{2Q} \right) + \gamma_{th,\ell}$ . Finally, by substituting (9) into (12), the average BLER of  $\bar{\epsilon}_{k,b}$  is obtained as

$$\bar{\epsilon}_{k,b} = 1 - 2\chi_k \sqrt{\mathcal{L}_k} \int_{\alpha_k}^{\beta_k} \sqrt{\Upsilon_k x} K_1(2\sqrt{\Upsilon_k x}) dx \quad (16)$$

where  $\Upsilon_k = \frac{1}{\lambda_{h_0} \lambda_{g_k} \delta \eta \rho_S}$ . Applying the Gaussian-Chebyshev quadrature,  $\bar{\epsilon}_{k,b}$  can be approximated as:

$$\begin{aligned} \bar{\epsilon}_{k,b} &\approx 1 - \frac{\chi_k \sqrt{\mathcal{L}_k} (\beta_k - \alpha_k) \pi}{Q} \\ &\quad \times \sum_{q=1}^Q \left| \sin \frac{(2q-1)\pi}{2Q} \right| \sqrt{\Upsilon_k \zeta_q} \\ &\quad \times K_1(2\sqrt{\Upsilon_k \zeta_q}). \end{aligned} \quad (17)$$

By substituting (17) and (15) into (13),  $\tilde{\varepsilon}_{U_k}$  is derived. The overall system throughput is represented as:

$$\tau_{\text{system}} = \sum_{k=1}^{\mathcal{K}} (1 - \tilde{\varepsilon}_{U_k}) R_k. \quad (18)$$

For convenience, all mathematical symbols introduced in Secs. 2 and 3 are also summarized in Tab. 2, facilitating easier cross-reference for readers and addressing the notation consistency requirement.

### 4. Results and Discussion

This section presents several numerical results to validate the information theoretic framework established in Sec. 3. All Monte-Carlo simulations were conducted in MATLAB R2023b with  $10^6$  independent iterations to ensure statistical accuracy. Unless otherwise specified, the baseline system parameters are summarized in Tab. 3. For each figure, one key parameter under investigation (e.g., transmit SNR, blocklength  $\mathcal{L}$ , power allocation  $a_c$ , reflection coefficient  $\delta$ , or efficiency coefficient  $\eta$ ) was varied, while the remaining parameters were fixed to their baseline values. This setup ensures a fair and consistent comparison of RSMA and NOMA performance across diverse URLLC short-packet scenarios. Different values of  $\mathcal{L} = \mathcal{L}_1 = \mathcal{L}_2 = \mathcal{L}_c$  were considered, and the Gauss-Chebyshev parameter was set to  $Q = 50$  to guarantee close numerical approximation, following [31].

The baseline power allocation coefficients ( $a_c = 0.3$ ,  $a_1 = 0.6(1 - a_c)$ , and  $a_2 = 0.4(1 - a_c)$ ) are selected following typical RSMA configurations reported in [4], [7], ensuring balanced interference management between the common and private streams. Moreover, to verify the generality of the proposed model, Figure 6 investigates the system throughput versus  $a_c$  for different blocklengths ( $\mathcal{L} = 200, 400, 600$ ), demonstrating that RSMA consistently outperforms NOMA and maintains robust performance across various allocation scenarios.

Figure 2 illustrates the average BLER performance of users in the RSMA system as a function of transmit SNR under different power allocation factors. As the SNR increases, the average BLER decreases, indicating improved communication reliability. This trend is expected because higher transmit power enhances signal strength and reduces decoding errors. In addition, user  $U_2$  experiences higher BLER than  $U_1$ , mainly due to differences in channel conditions and interference levels. Reducing the power allocation factor  $a_c$  yields significant improvements in BLER performance, particularly in low and medium SNR regimes. However, at very high SNR, the BLER improvement saturates, suggesting that power allocation alone may not further enhance reliability. The close agreement between analytical and simulation results validates the accuracy of the proposed theoretical model. Overall, Figure 2 demonstrates the impact of power allocation and SNR on system reliability, providing insights for optimizing RSMA-based URLLC systems.

Parameters	Values
Number of Monte-Carlo trials	$10^6$ iterations
Noise power	$N_0 = 1$ (normalized)
Power allocation	$a_c = 0.3$ $a_1 = 0.4(1 - a_c)$ $a_2 = 0.6(1 - a_c)$
Transmit SNR	$\rho_S = [0, \dots, 50]$ dB
Efficiency coefficient	$\delta = 0.3$
Reflection coefficient	$\eta = 0.8$
Blocklength	$\mathcal{L} = 400$ symbols
Number of information bits	$\mathcal{T}_1 = 100$ bits $\mathcal{T}_2 = \mathcal{T}_c = 80$ bits
Average channel gains	$\lambda_{h_0} = \lambda_{g_2} = 0.25$ $\lambda_{h_1} = \lambda_{g_1} = 0.5$ $\lambda_{h_2} = 0.75$ (normalized)

Note: The transmit SNR is defined as  $\rho_S = P_S/N_0$ , where  $P_S$  denotes the physical transmit power at the source node and  $N_0$  is the noise power spectral density. All units are explicitly indicated (SNR in dB, power in dBm or W, and coefficients are dimensionless).

Tab. 3. Simulation parameters [20], [30].

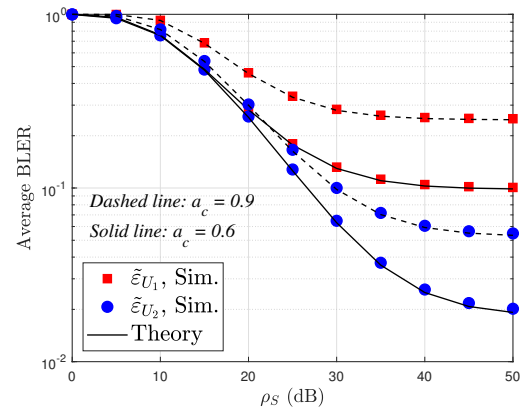


Fig. 2. Average BLER of  $U_k$  versus  $\rho_S$  in dB.

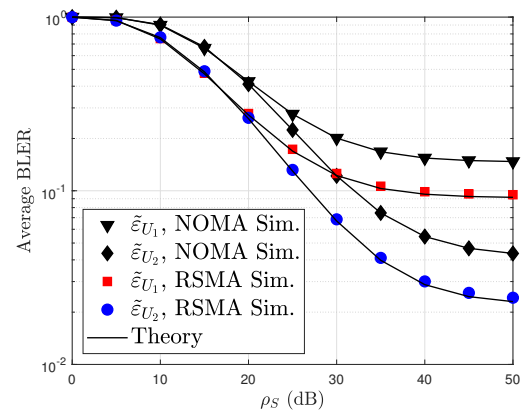


Fig. 3. Comparison between RSMA and NOMA for  $U_k$  with blocklength  $\mathcal{L} = 400$ , reflection efficiency  $\eta = 0.8$ , and coupling coefficient  $\delta = 0.3$ . Unless specified, power allocation factors are  $a_c = 0.3$ ,  $a_2 = 0.42$ , and  $a_1 = 0.28$ .

Figure 3 compares the average BLER performance of RSMA and NOMA under different SNR conditions. RSMA employs rate-splitting to divide messages into common and private parts, allowing users to decode their signals more efficiently, whereas NOMA relies on power-domain multi-

plexing and successive interference cancellation. The results indicate that RSMA achieves lower BLER than NOMA, demonstrating its superior reliability, particularly in high-interference scenarios. This improvement arises because RSMA effectively manages interference without requiring strong users to decode weak users' signals first, thus reducing decoding complexity and error propagation. Furthermore, RSMA provides improved fairness among users, as all users can decode a portion of the common message before handling their private messages, unlike NOMA, which favors strong users.

Figure 4 illustrates the relationship between the average BLER of users and the blocklength ( $\mathcal{L}$ ) in the RSMA system. Increasing the blocklength improves reliability by reducing BLER, as longer blocks enable more efficient error correction. However, this improvement comes at the cost of lower transmission rates because the number of transmitted information bits remains constant. In addition, higher transmit SNR enhances reliability further, reducing the required blocklength to meet a target reliability threshold. These results highlight the trade-off between latency, reliability, and spectral efficiency in short-packet transmissions.

Figure 5 compares the system throughput of RSMA and NOMA across different SNR values and blocklengths. RSMA consistently outperforms NOMA, particularly at higher SNR levels, owing to its superior interference management and efficient resource allocation. The throughput gain of RSMA becomes more pronounced when the blocklength is short, demonstrating its advantage in short-packet communication scenarios. These findings confirm that RSMA is a more effective multiple-access technique for optimizing spectral efficiency while maintaining reliability, making it suitable for URLLC applications requiring both high throughput and low latency.

In terms of computational cost, RSMA introduces only one additional common-message decoding step compared with NOMA, yielding comparable receiver complexity while maintaining better interference management.

Remark: The BLER curves in Figs. 2–4 reach a floor around  $10^{-3}$ – $10^{-4}$  because of the finite blocklength ( $\mathcal{L} = 400$ ) and the compounded fading of the ambient backscatter link. Achieving BLER values below  $10^{-5}$  would require unrealistically high transmit power or much longer packets, both incompatible with URLLC latency and energy constraints. The presented results therefore reflect the practical reliability bound of RSMA-backscatter short-packet transmissions while maintaining a consistent theoretical decreasing trend at higher SNRs.

Figure 6 presents the system throughput of RSMA and NOMA as a function of the power allocation factor  $a_c$  for different blocklengths  $\mathcal{L}$ . The throughput of both schemes increases with  $a_c$  up to an optimum point around 0.4–0.5, beyond which further increases in  $a_c$  reduce the private-stream rate and overall efficiency. Smaller blocklengths result in lower throughput due to limited coding gain, whereas

larger  $\mathcal{L}$  improves reliability. RSMA consistently surpasses NOMA for all blocklengths, confirming its throughput superiority and balanced interference management in URLLC short-packet communications.

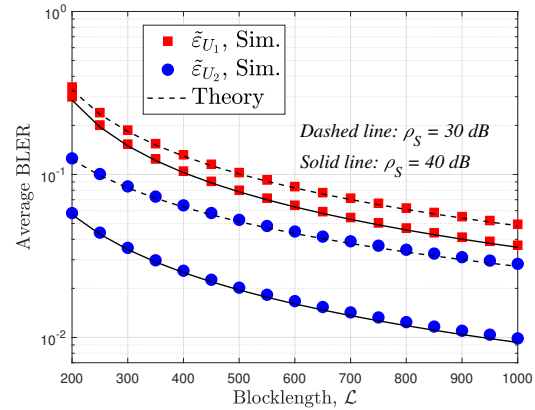


Fig. 4. Average BLER of  $U_k$  versus blocklength with reflection efficiency  $\eta = 0.8$ , and coupling coefficient  $\delta = 0.3$ . Unless specified, power allocation factors are  $a_c = 0.6$ ,  $a_2 = 0.24$ , and  $a_1 = 0.16$ .

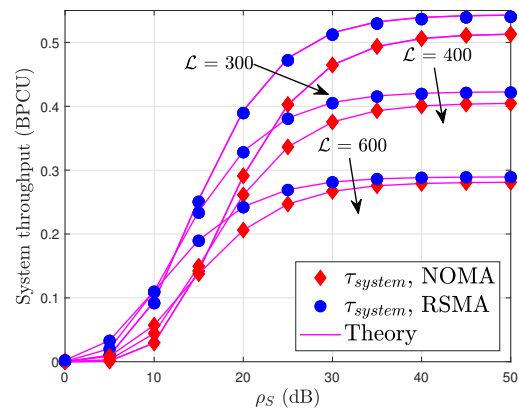


Fig. 5. System throughput versus  $\rho_S$  in dB with different  $\mathcal{L}$ , reflection efficiency  $\eta = 0.8$ , and coupling coefficient  $\delta = 0.3$ . Unless specified, power allocation factors are  $a_c = 0.3$ ,  $a_2 = 0.42$ , and  $a_1 = 0.28$ .

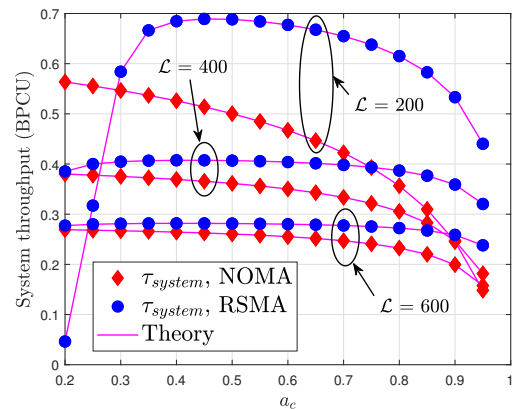
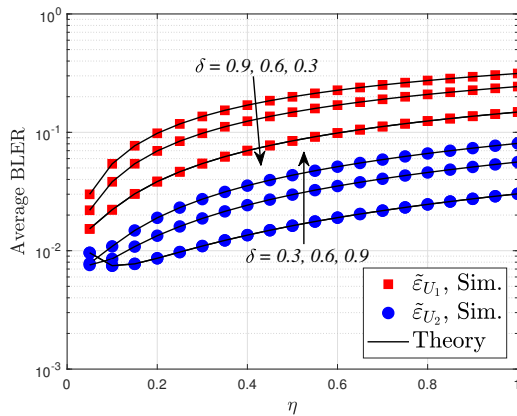
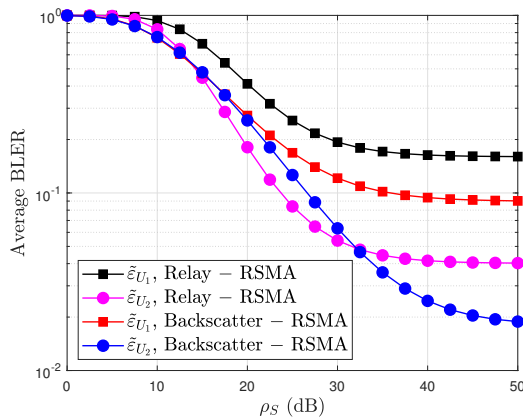


Fig. 6. System throughput versus  $a_c$  with different  $\mathcal{L}$ ,  $\rho_S = 30$  dB, reflection efficiency  $\eta = 0.8$ , and coupling coefficient  $\delta = 0.3$ . Unless specified, power allocation factors are  $a_2 = 0.6(1 - a_c)$ , and  $a_1 = 0.4(1 - a_c)$ .



**Fig. 7.** Average BLER of  $U_k$  versus reflection efficiency  $\eta$  with different  $\delta$ ,  $\rho_S = 50$  dB and blocklength  $\mathcal{L} = 500$ . Unless specified, power allocation factors are  $a_c = 0.8$ ,  $a_2 = 0.12$ , and  $a_1 = 0.08$ .



**Fig. 8.** Average BLER Comparison for Users in Relay-Assisted vs. Backscatter-Assisted Scenarios, with blocklength  $\mathcal{L} = 400$ , reflection efficiency  $\eta = 0.8$ , and coupling coefficient  $\delta = 0.3$ . Unless specified, power allocation factors are  $a_c = 0.5$ ,  $a_2 = 0.3$ , and  $a_1 = 0.2$ .

Figure 7 shows the impact of the reflection coefficient  $\delta$  and efficiency  $\eta$  on system reliability. As either  $\delta$  or  $\eta$  increases, the average BLER also increases, since stronger backscattered coupling intensifies the interference component at the users. The lowest BLER is achieved when both  $\delta$  and  $\eta$  are small, indicating that excessive reflection is detrimental to link reliability. This result highlights the trade-off between backscatter strength and interference in ambient RSMA systems.

Figure 8 presents a comparison between the proposed backscatter-assisted RSMA framework and a relay-assisted RSMA benchmark under identical simulation settings. The backscatter-assisted configuration achieves lower average BLER for both users in the medium-to-high SNR region. For instance, at  $\rho_S = 30$  dB, user  $U_2$  in the backscatter-assisted system achieves  $\bar{\epsilon}_{U_2} \approx 10^{-2}$ , while the relay-assisted counterpart yields  $\bar{\epsilon}_{U_2} \approx 10^{-1}$ , corresponding to roughly one order of magnitude improvement in reliability. This gain results from the symbiotic reuse of the base-station signal at the passive backscatter device, which enhances diversity

without the self-interference and power consumption inherent to full-duplex relaying [32]. At very high SNRs, both systems approach an interference-limited floor and the performance gap saturates. Overall, these results demonstrate that the proposed backscatter-assisted RSMA offers a favorable reliability-energy-efficiency trade-off compared with active cooperative RSMA, requiring zero transmit power and substantially reduced hardware complexity.

Note: The complete mathematical model and MATLAB simulation codes used in this study are available from the corresponding author upon reasonable request to facilitate result verification and further research.

## 5. Conclusion

This paper presented an analytical framework for evaluating the average block error rate (BLER) and throughput performance of an RSMA-enabled symbiotic backscatter (SB-RSMA) system under finite blocklength constraints for URLLC scenarios. Closed-form and approximate expressions were derived and validated via Monte Carlo simulations. The results showed that the proposed SB-RSMA framework achieves about one-order-of-magnitude lower BLER and 15–20% higher throughput than NOMA, confirming its superiority in reliability and spectral efficiency. Future work will extend this analytical framework to more complex fading models such as Rician (which includes a line-of-sight component as a special case of Rayleigh) and to scenarios with imperfect CSI and hardware impairments.

## References

- [1] MARAQA, O., RAJASEKARAN, A. S., AL-AHMADI, S., et al. A survey of rate-optimal power domain NOMA with enabling technologies of future wireless networks. *IEEE Communications Surveys & Tutorials*, 2020, vol. 22, no. 4, p. 2192–2235. DOI: 10.1109/COMST.2020.3013514
- [2] BUDHIRAJA, I., KUMAR, N., TYAGI, S., et al. A systematic review on NOMA variants for 5G and beyond. *IEEE Access*, 2021, vol. 9, p. 85573–85644. DOI: 10.1109/ACCESS.2021.3081601
- [3] LUU, B.-H., LAM, S.-C., NGUYEN, N.-H., et al. Performance of the user in the TDD NOMA cellular networks enabling FFR. *Radioengineering*, 2024, vol. 33, no. 2, p. 312–321. DOI: 10.13164/re.2024.0312
- [4] MAO, Y., DIZDAR, O., CLERCKX, B., et al. Rate-splitting multiple access: Fundamentals, survey, and future research trends. *IEEE Communications Surveys & Tutorials*, 2022, vol. 24, no. 4, p. 2073–2126. DOI: 10.1109/COMST.2022.3191937
- [5] ZHOU, G., MAO, Y., CLERCKX, B. Rate-splitting multiple access for multi-antenna downlink communication systems: Spectral and energy efficiency tradeoff. *IEEE Transactions on Wireless Communications*, 2022, vol. 21, no. 7, p. 4816–4828. DOI: 10.1109/TWC.2021.3133433
- [6] JAAFAR, W., NASER, S., MUHAIDAT, S., et al. On the downlink performance of RSMA-based UAV communications. *IEEE Transactions on Vehicular Technology*, 2020, vol. 69, no. 12, p. 16258–16263. DOI: 10.1109/TVT.2020.3037657

- [7] SOLEYMANI, M., SANTAMARIA, I., JORSWIECK, E., et al. Optimization of rate-splitting multiple access in beyond diagonal RIS-assisted URLLC systems. *IEEE Transactions on Wireless Communications*, 2024, vol. 23, no. 5, p. 5063–5078. DOI: 10.1109/TWC.2023.3324190
- [8] DE SENA, A. S., NARDELLI, P. H. J., DA COSTA, D. B. Rate-splitting multiple access and its interplay with intelligent reflecting surfaces. *IEEE Communications Magazine*, 2022, vol. 60, no. 7, p. 52–57. DOI: 10.1109/MCOM.004.2100956
- [9] LYU, X., ADITYA, S., KIM, J., et al. Rate-splitting multiple access: The first prototype and experimental validation of its superiority over SDMA and NOMA. *IEEE Transactions on Wireless Communications*, 2024, vol. 23, no. 8, p. 9986–10000. DOI: 10.1109/TWC.2024.3367891
- [10] NGUYEN, V.-S., LE-THI, A., VU, D.-T., et al. Analysis of ergodic sum rate in RSMA with perfect and imperfect SIC: A multiple-antenna selection approach for optimizing UAV positioning. *Physical Communication*, 2025, vol. 72, p. 1–11. DOI: 10.1016/j.phycom.2025.102741
- [11] MOLOUDIAN, G., JAFARI, R., KIM, H., et al. RF energy harvesting techniques for battery-less wireless sensing, Industry 4.0, and Internet of Things: A review. *IEEE Sensors Journal*, 2024, vol. 24, no. 5, p. 5732–5745. DOI: 10.1109/JSEN.2024.3352402
- [12] XU, Y., WANG, M., JIA, Y., et al. Robust beamforming and rate optimization for RIS-aided symbiotic radio systems with RSMA. *IEEE Communications Letters*, 2024, vol. 28, no. 10, p. 2328–2332. DOI: 10.1109/LCOMM.2024.3451700
- [13] WANG, Z., WANG, Q., DANG, X. Altitude range and throughput analysis for directional UAV-assisted BackCom networks. *Radioengineering*, 2024, vol. 33, no. 3, p. 368–375. DOI: 10.13164/re.2024.0368
- [14] ONAY, M. Y., ERTUG, O. Ambient backscatter communication based cooperative relaying for heterogeneous cognitive radio networks. *Radioengineering*, 2023, vol. 32, no. 2, p. 236–247. DOI: 10.13164/re.2023.0236
- [15] AURANGZEB, M. H., AKRAM, F., RASHID, I., et al. Pilots optimization and surface area effects on channel estimation in RIS-aided MIMO system. *Radioengineering*, 2023, vol. 32, no. 2, p. 187–196. DOI: 10.13164/re.2023.0187
- [16] DO, Q. V., VU, M. B., NGUYEN, Q.-S., et al. Analysis of symbiotic backscatter empowered wireless sensors network with short-packet communications. *PLOS One*, 2024, vol. 19, no. 8, p. 1–17. DOI: 10.1371/journal.pone.0307366
- [17] NGUYEN, Q.-S., LE ANH, U.-V., NGUYEN, T. N., et al. Short-packet communications for relay systems with co-channel interference at relay: Performance analysis and power control. *IEEE Access*, 2024, vol. 12, p. 63452–63461. DOI: 10.1109/ACCESS.2024.3396642
- [18] NGUYEN, Q.-S., KIM, H.-Y., NGUYEN, T. N., et al. Performance of RIS-secured short-packet NOMA systems with discrete phase-shifter to protect digital content and copyright against untrusted user. *IEEE Access*, 2025, vol. 13, p. 21580–21593. DOI: 10.1109/ACCESS.2025.3535813
- [19] XU, Y., MAO, Y., DIZDAR, O., et al. Rate-splitting multiple access with finite blocklength for short-packet and low-latency downlink communications. *IEEE Transactions on Vehicular Technology*, 2022, vol. 71, no. 11, p. 12333–12337. DOI: 10.1109/TVT.2022.3191085
- [20] VU, T.-H., DA COSTA, D. B., NGUYEN, B. V. N. Q., et al. A novel paradigm shift for next-generation: symbiotic backscatter rate-splitting multiple access systems. In *Proceedings of the IEEE 10th International Conference on Communications and Electronics (ICCE)*. Da Nang (Vietnam), 2024, p. 1–6. DOI: 10.1109/ICCE62051.2024.10634646
- [21] ABD-ALAZIZ, W., ABOOD, B., MUTTASHER, R. M., et al. Exact BER performance analysis of an elementary coding technique for NOMA system on AWGN channel. *Radioengineering*, 2024, vol. 33, no. 1, p. 45–53. DOI: 10.13164/re.2024.0045
- [22] CHEN, Y., LU, H., WU, C., et al. Performance optimization in RSMA-assisted uplink xURLLC IIoT networks with statistical QoS provisioning. *IEEE Transactions on Wireless Communications*, Early Access, 2025, p. 1–15. DOI: 10.1109/TWC.2025.3577694
- [23] SEYFI, M., MUHAIDAT, S., LIANG, J., et al. Relay selection in dual-hop vehicular networks. *IEEE Signal Processing Letters*, 2011, vol. 18, no. 2, p. 134–137. DOI: 10.1109/LSP.2010.2102017
- [24] LE, C.-B., PHAN, H.-L., NGUYEN, T.-N., et al. Joint design of improved spectrum and energy efficiency with backscatter NOMA for IoT. *IEEE Access*, 2021, vol. 10, p. 7504–7519. DOI: 10.1109/ACCESS.2021.3139118
- [25] GRADSHTEYN, I. S., RYZHIK, I. M. *Table of Integrals, Series and Products*. 6th ed. New York (USA): Academic Press, 2000. ISBN: 9780122947575
- [26] POLYANSKIY, Y., POOR, H. V., VERDU, S. Channel coding rate in the finite block-length regime. *IEEE Transactions on Information Theory*, 2010, vol. 56, no. 5, p. 2307–2359. DOI: 10.1109/TIT.2010.2043769
- [27] YUAN, L., DU, Q., FANG, F. Performance analysis of full-duplex cooperative NOMA short-packet communications. *IEEE Transactions on Vehicular Technology*, 2022, vol. 71, no. 12, p. 13409–13414. DOI: 10.1109/TVT.2022.3199541
- [28] XIA, C., XIANG, Z., SU, B., et al. RIS-NOMA assisted short-packet communication with hardware impairments. *IEEE Internet of Things Journal*, 2024, vol. 11, no. 2, p. 2990–3002. DOI: 10.1109/JIOT.2023.3337698
- [29] ABRAMOWITZ, M., STEGUN, I. A. *Handbook of Mathematical Functions With Formulas, Graphs, and Mathematical Tables*. New York (USA): Dover, 1972. ISBN: 9780486612720
- [30] NGUYEN, T.-T.-T., NGUYEN, X.-X. Average block error rate analysis of IRS-aided NOMA short-packet communication systems. In *Proceedings of the International Symposium on Electrical and Electronics Engineering (ISEE)*. Ha Noi (Vietnam), 2023, p. 91–96. DOI: 10.1109/ISEE59483.2023.10299877
- [31] CHENG, Y., LI, K. H., LIU, Y., et al. Downlink and uplink intelligent reflecting surface aided networks: NOMA and OMA. *IEEE Transactions on Wireless Communications*, 2021, vol. 20, no. 6, p. 3988–4000. DOI: 10.1109/TWC.2021.3054841
- [32] KHISA, S., ALMEKHLAFI, M., ELHATTAB, M., et al. Full-duplex cooperative rate-splitting multiple access for a MISO broadcast channel with two users. *IEEE Communications Letters*, 2022, vol. 26, no. 8, p. 1913–1917. DOI: 10.1109/LCOMM.2022.3173894

## About the Authors ...

**Anh Thu PHAN** received a B.E. degree in Telecommunication Engineering from the Posts and Telecommunications Institute of Technology (PTIT), Viet Nam, in 2003, and M.E. degree in Telecommunication Engineering from Royal Melbourne Institute of Technology, Australia, in 2008. She received the Ph.D. degree in Telecommunication Engineering from PTIT in 2010. Now, she is a Lecturer at the telecommunication faculty of PTIT. Her research interests include networking, radio over fiber, and broadband networks.

**Sang-Quang NGUYEN** received the B.E. degree in Electrical Engineering from Ho Chi Minh City University of Transport, Vietnam, in 2010, the M.E. degree in Telecommunications Engineering from Ho Chi Minh City University of Technology, Vietnam, in 2013, and the Ph.D. degree in Electrical Engineering from the University of Ulsan, South Korea, in 2017. From 2017 to 2021, he was a Lecturer at Duy Tan University, Vietnam. Since May 2021, he has been a Lecturer at Ho Chi Minh City University of Transport, Vietnam. In September 2024, he joined the Post and Telecommunications Institute of Technology, Ho Chi Minh City, as a Lecturer. He also served as a Research Fellow at Queen's University Belfast, United Kingdom, where he contributed to advancements in wireless communications. Dr. Sang's research interests include cooperative communications, cognitive radio networks, physical layer security, non-orthogonal multiple access (NOMA), short-packet communications, and backscatter communications. His work primarily focuses on secure and energy-efficient communication solutions for next-generation wireless networks. Dr. Sang can be contacted via email at sangnq@ptit.edu.vn.

**Phu-Nguyen LE** received a B.S. degree in Electrical Engineering from Da Nang University of Technology, Da Nang, Vietnam, in 2012. He received his Ph.D. degree in the School of Electrical Engineering, University of Ulsan, Ulsan, South Korea in 2021. He is currently a Lecturer in Faculty of Engineering and Technology, Nguyen Tat Thanh University. His research interests include sensor-based robotic applications, robot calibration, and artificial intelligent-based robotic calibration.

**Hai Trieu LE** was born in Vietnam. He received his M.Sc. degree from the Institute of Science and Technology, Ministry of Public Security (MoPS), Vietnam. His research interests include ambient backscatter communications, energy harvesting techniques, and wireless sensor networks for security applications.

**Minh Tuan DANG** received his Ph.D. in Mathematics in 2017. He has 19 years of experience in Automation and nearly 20 years in Information Technology. Currently, he is the Director of the CMC Applied Technology Institute (since 2019) and Head of the Department of Microelectronics and Telecommunications at CMC University since 2024. His research focuses on 5G/6G networks, physical layer security, and URLLC. He has published extensively on security mechanisms for next-generation wireless networks and secure IoT communication frameworks.

**Trong Minh HOANG** (corresponding author) (Senior Member, IEEE) received the Ph.D degree in Telecommunication Engineering (2014) from Posts and Telecommunications Institute of Technology. He is currently an Associate Professor in the Telecommunication Faculty of Posts and Telecommunications Institute of Technology. He is the Head of the Telecommunication Network Department and the Head of the Intelligent Connected Networks Laboratory. He has been working on the issues surrounding the performance of wireless networks. His research interests include network performance and security issues in edge computing, wireless mobile networks, and 5G/6G networks. He is a member of the IEEE and IEEE Circuits and Systems Society.